Extracellular matrix stiffness and TGFβ2 regulate YAP/TAZ activity in human trabecular meshwork cells

Haiyan Li[a,b,c], VijayKrishna Raghunathan[d], W. Daniel Stamer[e,f], Preethi S. Ganapathy[a,c,g], Samuel Herberg[a,b,c,h,i*]

Affiliations:
[a] Department of Ophthalmology and Visual Sciences, SUNY Upstate Medical University, Syracuse, NY 13210, USA
[b] Department of Cell and Developmental Biology, SUNY Upstate Medical University, Syracuse, NY 13210, USA
[c] BioInspired Institute, Syracuse University, Syracuse, NY 13244, USA
[d] Department of Basic Sciences, The Ocular Surface Institute, University of Houston, Houston, TX 77204, USA
[e] Department of Ophthalmology, Duke Eye Center, Duke University, Durham, NC 27708, USA
[f] Department of Biomedical Engineering, Duke University, Durham, NC 27708, USA
[g] Department of Neuroscience and Physiology, SUNY Upstate Medical University, Syracuse, NY 13210, USA
[h] Department of Biochemistry and Molecular Biology, SUNY Upstate Medical University, Syracuse, NY 13210, USA
[i] Department of Biomedical and Chemical Engineering, Syracuse University, Syracuse, NY 13244, USA

*To whom correspondence should be addressed: Samuel Herberg, PhD, Assistant Professor; Department of Ophthalmology and Visual Sciences, SUNY Upstate Medical University, 505 Irving Avenue, Neuroscience Research Building Room 4609, Syracuse, NY 13210, USA, email: herbergs@upstate.edu

Keywords: Mechanotransduction, hydrogel, HTM cell contractility, HTM stiffness, POAG

Abstract

Primary open-angle glaucoma progression is associated with increased human trabecular meshwork (HTM) stiffness and elevated transforming growth factor beta 2 (TGFβ2) levels in aqueous humor. Increased transcriptional activity of Yes-associated protein (YAP) and transcriptional coactivator with PDZ-binding motif (TAZ), central players in mechanotransduction, are implicated in glaucomatous HTM cell dysfunction. Yet, the detailed mechanisms underlying YAP/TAZ modulation in HTM cells in response to alterations in extracellular matrix (ECM) stiffness and TGFβ2 levels are not well understood. Using biomimetic ECM hydrogels with tunable stiffness, here we show that increased ECM stiffness elevates YAP/TAZ transcriptional activity potentially through modulating focal adhesions and cytoskeletal rearrangement. Furthermore, TGFβ2 increased YAP/TAZ nuclear localization in both normal and glaucomatous HTM cells, which was prevented by inhibiting extracellular-signal-regulated kinase and Rho-associated kinase signaling pathways to varying degrees. Filamentous (F)-actin depolymerization reversed TGFβ2-induced YAP/TAZ nuclear localization. YAP/TAZ depletion using siRNA or verteporfin decreased focal adhesions, ECM remodeling and cell contractile properties. Similarly, YAP/TAZ inactivation with simvastatin or verteporfin partially blocked TGFβ2-induced HTM hydrogel contraction and stiffening. Collectively, our data provide strong evidence for a pathologic role of aberrant YAP/TAZ signaling in glaucomatous HTM cell dysfunction, and may help inform strategies for the development of novel multifactorial approaches to prevent progressive ocular hypertension in glaucoma.

1. Introduction

Primary open-angle glaucoma (POAG) is a leading cause of irreversible vision loss worldwide, and elevated intraocular pressure (IOP) is the primary modifiable risk factor [1-5]. Elevated IOP results from increased resistance to aqueous humor outflow at the trabecular meshwork (TM) [6]. Human trabecular meshwork (HTM) cells within the tissue are surrounded by a complex extracellular matrix (ECM), which is primarily composed of non-fibrillar and fibrillar collagens, elastic fibrils, proteoglycans and the glycosaminoglycan hyaluronic acid [7-11]. In addition to providing structural support, the ECM imparts biochemical signals (e.g., hormones, growth factors and diffusible morphogens) and mechanical cues (e.g., matrix stiffness; tensile, compressive and shear forces; topographical strain) to regulate cell behaviors [12]. These external biophysical cues are translated into internal biochemical signaling cascades through a process known as mechanotransduction, and cells play an active role in remodeling their matrix to promote mechanical homeostasis and maintain tissue-level functionality [13].

HTM cells are exposed to a variety of biophysical cues through cell-cell and cell-ECM interactions, and fluctuations in IOP. In POAG, impaired HTM cell function (i.e., remodeling of cell cytoskeleton, increased cell stiffness) and increased ECM deposition contribute to HTM stiffening [14-17]. HTM stiffening affects HTM cell function, and IOP in a feed-forward cycle characterized by dynamic reciprocity. The correlation between HTM stiffening and POAG indicates that a biophysical component likely contributes to IOP regulation. Therefore, targeting mechanotransduction pathways in the HTM by interrupting this potential feed-forward cycle between HTM stiffening and cellular response to the stiffened ECM is emerging as a promising strategy for managing ocular hypertension.

Yes-associated protein (YAP) and transcriptional coactivator with PDZ-binding motif (TAZ, encoded by WWTR1) are central players in mechanotransduction. YAP/TAZ can be activated by increased ECM stiffness, mechanical stress and growth factors [18, 19]. It has been demonstrated that certain glaucoma related molecules that influence outflow function, such as dexamethasone, lysophosphatidic acid and interleukin-6, mediate the expression of YAP and TAZ in HTM cells [20-22]. YAP was found to be reduced in HTM cells incubated on stiff two-dimensional (2D) polyacrylamide hydrogels, while TAZ levels were increased [23]. On the contrary, other research showed that both YAP and TAZ were significantly higher in HTM cells on stiffer polyacrylamide substrates or stiffened HTM cell-derived matrices [24, 25]. Together, this suggests that the precise role of YAP/TAZ in HTM mechanotransduction is far from clear. The noted substrate and context dependency of YAP/TAZ signaling highlights the importance of utilizing a better mimic of the native tissue to further our understanding of HTM cell mechanobiology with focus on cell-ECM interactions.

Biomaterials for cell culture applications are designed to mimic aspects of the ECM and provide researchers with methods to better understand cell behaviors. Protein-based hydrogels (i.e., water-swollen networks of polymers) are attractive biomaterials owing to their similarity to *in vivo* cellular microenvironments, biocompatibility, biodegradability and tunable mechanical properties [26, 27]. Recently, we developed a bioengineered hydrogel composed of HTM cells and ECM biopolymers found in the native HTM tissue, and demonstrated its viability for investigating cell-ECM interactions under normal and simulated glaucomatous conditions in both 2D and 3D conformations [17, 28].

Here, we hypothesized that elevated YAP/TAZ transcriptional activity drives HTM cell dysfunction under simulated glaucomatous conditions. The HTM from POAG eyes is stiffer than

that from healthy eyes [29-31]; transforming growth factor beta 2 (TGFβ2), the predominant TGFβ isoform in the eye and aqueous humor, has been identified as a major contributor to the pathologic changes occurring in ocular hypertension and POAG [1, 32-36]. Using TGFβ2 as a glaucomatous stimulus and tuning the stiffness of our hydrogels, here, we investigated the effects of TGFβ2 and ECM stiffness on regulating YAP/TAZ transcriptional activity in HTM cells in 2D and 3D cultures. In this tissue-mimetic environment, we then investigated whether YAP/TAZ inhibition would alleviate ECM stiffness- or TGFβ2-induced HTM cell pathobiology.

2. Materials and Methods

2.1 HTM cell isolation and culture.

Human donor eye tissue use was approved by the SUNY Upstate Medical University Institutional Review Board (protocol #1211036), and all experiments were performed in accordance with the tenets of the Declaration of Helsinki for the use of human tissue. Primary HTM cells were isolated from healthy donor corneal rims discarded after transplant surgery as recently described [17, 28], and cultured according to established protocols [37, 38]. Four HTM cell strains (HTM05, HTM12, HTM14, HTM19) were used for the experiments in this study (HTM cell strain information can be found in **Suppl. Table. 1**). All HTM cell strains were validated with dexamethasone (DEX; Fisher Scientific, Waltham, MA, USA; 100 nM) induced myocilin (MYOC) expression in more than 50% of cells by immunocytochemistry and immunoblot analyses (**Suppl. Fig. 1A,B** and [17, 28]). Different combinations of 2-3 HTM cell strains were used per experiment with 3-4 replicates each, depending on cell availability, and all studies were conducted between cell passage 3-7. HTM cells were cultured in low-glucose Dulbecco's Modified Eagle's Medium (DMEM; Gibco; Thermo Fisher Scientific) containing 10% fetal bovine serum (FBS; Atlanta

Biologicals, Flowery Branch, GA, USA) and 1% penicillin/streptomycin/glutamine (PSG; Gibco), and maintained at 37°C in a humidified atmosphere with 5% CO_2. Fresh media was supplied every 2-3 days.

2.2 Glaucomatous donor history

Donor was a 75-year-old, white female that was taking Xalatan (0.005%) in both eyes nightly for treatment of ocular hypertension. The patient was diagnosed with glaucoma, and had bilateral cataract surgery, and retina surgery. Upon receipt of donor eyes by W.D.S., outflow facility measurements during constant pressure perfusion conditions were 0.24 and 0.17 µl/min/mmHg from OD and OS eyes, respectively. Glaucomatous HTM cells (GTM211) were isolated from the OS eye of the donor and characterized as previously described [17]. GTM211 and GTM1445 (characterized in **Suppl. 1C,D** and [17]) were used in this study (GTM cell strain information can be found in **Suppl. Table. 1**).

2.3 Preparation of hydrogels.

Hydrogel precursors methacrylate-conjugated bovine collagen type I (MA-COL, Advanced BioMatrix, Carlsbad, CA, USA; 3.6 mg/ml [all final concentrations]), thiol-conjugated hyaluronic acid (SH-HA, Glycosil®, Advanced BioMatrix; 0.5 mg/ml, 0.025% (w/v) photoinitiator Irgacure® 2959; Sigma-Aldrich, St. Louis, MO, USA) and in-house expressed elastin-like polypeptide (ELP, thiol via KCTS flanks [17]; 2.5 mg/ml) were thoroughly mixed. Thirty microliters of the hydrogel solution were pipetted onto a Surfasil (Fisher Scientific) coated 12-mm round glass coverslip followed by placing a regular 12-mm round glass coverslip onto the hydrogels. Constructs were crosslinked by exposure to UV light (OmniCure S1500 UV Spot Curing System; Excelitas

Technologies, Mississauga, Ontario, Canada) at 320-500 nm, 2.2 W/cm^2 for 5 s, as previously described [17]. The hydrogel-adhered coverslips were removed with fine-tipped tweezers and placed in 24-well culture plates (Corning; Thermo Fisher Scientific). Hydrogel stiffening was achieved by soaking the hydrogels in 0.1% (w/v) riboflavin (RF; Sigma) for 5 min, followed by low-intensity secondary UV crosslinking (bandpass filter: 405-500 nm, 5.4 mW/cm^2) for 5 min.

2.4 HTM cell treatments.

HTM/GTM cells were seeded at 2 × 10^4 cells/cm^2 on premade hydrogels/coverslips/tissue culture plates, and cultured in DMEM with 10% FBS and 1% PSG for 1 or 2 days. Then, HTM cells were cultured in serum-free DMEM with 1% PSG and subjected to the different treatments for 3 d: TGFβ2 (2.5 ng/ml; R&D Systems, Minneapolis, MN, USA), the ERK inhibitor U0126 (10 μM; Promega, Madison, WI, USA), the Rho-associated kinase (ROCK) inhibitor Y27632 (10 μM; Sigma-Aldrich), the actin de-polymerizer latrunculin B (10 μM; Tocris Bioscience; Thermo Fisher Scientific), the YAP inhibitor verteporfin (0.5 μM; Sigma), or the HMG-CoA reductase inhibitor simvastatin (10 μM; Sigma). The monolayer HTM cells were processed for immunoblot, qRT-PCR and immunocytochemistry analyses.

2.5 Immunoblot analysis.

Protein was extracted from cells using lysis buffer (CelLytic™ M, Sigma-Aldrich) supplemented with Halt™ protease/phosphatase inhibitor cocktail (Thermo Fisher Scientific). Equal protein amounts (10 μg), determined by standard bicinchoninic acid assay (Pierce; Thermo Fisher Scientific), in 4× loading buffer (Invitrogen; Thermo Fisher Scientific) with 5% beta-mercaptoethanol (Fisher Scientific) were boiled for 5 min and subjected to SDS-PAGE using

NuPAGE™ 4-12% Bis-Tris Gels (Invitrogen; Thermo Fisher Scientific) at 120V for 80 min and transferred to 0.45 µm PVDF membranes (Sigma; Thermo Fisher Scientific). Membranes were blocked with 5% bovine serum albumin (Thermo Fisher Scientific) in tris-buffered saline with 0.2% Tween®20 (Thermo Fisher Scientific), and probed with various primary antibodies followed by incubation with HRP-conjugated secondary antibodies or fluorescent secondary antibodies (LI-COR, Lincoln, NE, USA). Bound antibodies were visualized with the enhanced chemiluminescent detection system (Pierce) on autoradiography film (Thermo Fisher Scientific) or Odyssey® CLx imager (LI-COR). Densitometry was performed using the open-source National Institutes of Health software platform, FIJI [39] or Image Studio™ Lite (LI-COR); data were normalized to GAPDH. A list of all of antibodies used in this study, including their working dilutions, can be found in **Supplementary Table 2**.

2.6 Immunocytochemistry analysis.

HTM cells in presence of the different treatments were fixed with 4% paraformaldehyde (Thermo Fisher Scientific) at room temperature for 20 min, permeabilized with 0.5% Triton™ X-100 (Thermo Fisher Scientific), blocked with blocking buffer (BioGeneX), and incubated with primary antibodies, followed by incubation with fluorescent secondary antibodies; nuclei were counterstained with 4′,6′-diamidino-2-phenylindole (DAPI; Abcam). Similarly, cells were stained with Phalloidin-iFluor 488 (Abcam)/DAPI according to the manufacturer's instructions. Coverslips were mounted with ProLong™ Gold Antifade (Invitrogen) on Superfrost™ microscope slides (Fisher Scientific), and fluorescent images were acquired with an Eclipse N*i* microscope (Nikon Instruments, Melville, NY, USA). Fluorescent signal intensity was measured using FIJI

software. A list of all of antibodies used in this study, including their working dilutions, can be found in **Supplementary Table 2**.

2.7 Image analysis

All image analysis was performed using FIJI software. Briefly, YAP/TAZ localization were measured by quantifying the number of cells with higher intensity signal in the nucleus than cytoplasm, followed by calculating percent cellular localization N > C and N ≤ C. The cytoplasmic YAP intensity was measured by subtracting the overlapping nuclear (DAPI) intensity from the total YAP intensity. The nuclear YAP intensity was recorded as the proportion of total YAP intensity that overlapped with the nucleus (DAPI). YAP/TAZ nuclear/cytoplasmic (N/C) ratio was calculated as follows: N/C ratio = (nuclear YAP signal/area of nucleus)/(cytoplasmic signal/area of cytoplasm). Fluorescence intensity of F-actin, αSMA, FN, and p-MLC, and number of vinculin puncta were measured in at least 20 images from 2 HTM cell strains with 3 biological replicates per HTM cell strain with image background subtraction using FIJI software. Nuclear area was also measured using FIJI software. At least 100 nuclei were analyzed from 2 HTM cell strains with 3 biological replicates per HTM cell strain.

2.8 Quantitative reverse transcription-polymerase chain reaction (qRT-PCR) analysis.

Total RNA was extracted from HTM cells using PureLink RNA Mini Kit (Invitrogen). RNA concentration was determined with a NanoDrop spectrophotometer (Thermo Fisher Scientific). RNA was reverse transcribed using iScript™ cDNA Synthesis Kit (BioRad, Hercules, CA, USA). One hundred nanograms of cDNA were amplified in duplicates in each 40-cycle reaction using a CFX 384 Real Time PCR System (BioRad) with annealing temperature set at 60ºC, Power

SYBR™ Green PCR Master Mix (Thermo Fisher Scientific), and custom-designed qRT-PCR primers. Transcript levels were normalized to GAPDH, and mRNA fold-changes calculated relative to vehicle controls using the comparative C_T method [40]. A list of all of primers used in this study can be found in **Supplementary Table 3**.

2.9 Active TGFβ2 enzyme-linked immunosorbent assay (ELISA).

Total TGFβ levels were quantified using the Quantikine ELISA kit (R&D Systems). HTM and GTM cells were seeded at 2×10^4 cells/cm^2 on tissue culture plates, and cultured in DMEM with 10% FBS and 1% PSG for 1 or 2 days to grow to 80 – 90 % confluence. Then, HTM and GTM cells were cultured in 1 ml serum-free DMEM with 1% PSG for 3 d. After 3 days, the cell culture supernatants were collected and centrifuged at 1000 g for 10 min. The supernatants were used for ELISA according to the manufacturer's instructions.

2.10 siRNA transfection

HTM cells were depleted of YAP and TAZ using siRNA-loaded lipofectamine RNAimax (Invitrogen) according to the manufacturer's instructions. In brief, HTM cells were seeded at 2×10^4 cells/cm^2 on RF mediated double-crosslinked hydrogels in DMEM with 10% FBS and 1% PSG. The following day, the cell culture medium was changed to antibiotic-free and serum-free DMEM and the samples were kept in culture for 24 h followed by transfection. Transfection was performed using a final concentration 3% (v/v) lipofectamine RNAimax with 150 nM RNAi duplexes (custom oligonucleotides; Dharmacon). Transfected HTM cells were used 48 h after transfection. ON-TARGET plus nontargeting siRNA were obtained from Dharmacon. Custom siRNA were based on sequences previously described [18]: YAP, sense, 5'-

GACAUCUUCUGGUCAGAGA-3', and YAP, anti-sense, 5'-UCUCUGACCAGAAGAUGUC-3'; TAZ, sense, 5'-ACGUUGACUUAGGAACUUU-3', and TAZ, anti-sense, 5'-AAAGUUCCUAAGUCAACGU-3'.

2.11 *HTM hydrogel contraction analysis.*

HTM cell-laden hydrogels were prepared by mixing HTM cells (1.0×10^6 cells/ml) with MA-COL (3.6 mg/ml [all final concentrations]), SH-HA (0.5 mg/ml, 0.025% (w/v) photoinitiator) and ELP (2.5 mg/ml) on ice, followed by pipetting 10 µl droplets of the HTM cell-laden hydrogel precursor solution onto polydimethylsiloxane-coated (Sylgard 184; Dow Corning) 24-well culture plates. Constructs were crosslinked as described above (320-500 nm, 2.2 W/cm^2, 5 s). HTM cell-laden hydrogels were cultured in DMEM with 10% FBS and 1% PSG in presence of the different treatments. Longitudinal brightfield images were acquired at 0 d and 5 d with an Eclipse T*i* microscope (Nikon). Construct area from N = 8-11 hydrogels per group from 2 HTM/GTM cell strains with 3-4 biological replicates per HTM/GTM cell strain was measured using FIJI software and normalized to 0 d followed by normalization to controls.

2.12 HTM hydrogel cell proliferation analysis.

Cell proliferation was measured with the CellTiter 96® Aqueous Non-Radioactive Cell Proliferation Assay (Promega) following the manufacturer's protocol. HTM hydrogels cultured in DMEM with 10% FBS and 1% PSG in presence of the different treatments for 5 d were incubated with the staining solution (38 µl MTS, 2 µl PMS solution, 200 µl DMEM) at 37ºC for 1.5 h. Absorbance at 490 nm was recorded using a spectrophotometer plate reader (BioTEK, Winooski, VT, USA). Blank-subtracted absorbance values served as a direct measure of HTM cell

proliferation from N = 6-8 hydrogels per group from 2 HTM/GTM cell strains with 3-4 biological replicates per HTM/GTM cell strain.

2.13 HTM hydrogel rheology analysis.

Fifty microliters of acellular hydrogel precursor solutions were pipetted into custom 8x1-mm PDMS molds. Similarly, 250 µl of HTM cell-laden hydrogel precursor solutions were pipetted into 16x1-mm PDMS molds. All samples were UV crosslinked and equilibrated as described above. Acellular hydrogels were measured at 0 d. HTM hydrogels, cultured in DMEM with 10% FBS and 1% PSG in presence of the different treatments, were measured at 5 d; samples were cut to size using an 8-mm diameter tissue punch. A Kinexus rheometer (Malvern Panalytical, Westborough, MA, USA) fitted with an 8-mm diameter parallel plate was used to measure hydrogel viscoelasticity. To ensure standard conditions across all experiments (N = 3 per group), the geometry was lowered into the hydrogels until a calibration normal force of 0.02 N was achieved. Subsequently, an oscillatory shear-strain sweep test (0.1-60%, 1.0 Hz, 25°C) was applied to determine storage modulus (G') and loss modulus (G") in the linear region. Elastic modulus was calculated with $E = 2 * (1 + v) * G'$, where a Poisson's ratio (v) of 0.5 for the ECM hydrogels was assumed [41].

2.14 HTM hydrogel atomic force microscopy (AFM) analysis.

Thirty microliters of HTM cell-laden hydrogels solution were pipetted onto a Surfasil (Fisher Scientific) coated 12-mm round glass coverslip followed by placing a regular 12-mm round glass coverslip onto the hydrogels. Constructs were crosslinked by exposure to UV light at 320-500 nm, 2.2 W/cm^2 for 5 s, and cultured in DMEM with 10% FBS and 1% PSG for 7 days. Samples were

shipped overnight to UHCO where they were locally masked. Elastic modulus of HTM cell-laden hydrogels were obtained by atomic force microscopy (AFM) in fluid in contact mode as described previously [42]. Briefly, force vs. indentation curves were obtained on a Bruker BioScope Resolve (Bruker nanoSurfaces, Santa Barbara, CA) AFM employing a PNP-TR cantilever (NanoAndMore, Watsonville, CA) whose pyramidal tip was modified with a borosilicate bead (nominal diameter 5 μm), nominal spring constant of 0.32 N/m assuming sample Poisson's ratio of 0.5. The diameter of each sphere attached to the cantilever was qualified prior to usage. Prior to experimental samples, cantilever was calibrated on a silicon wafer in fluid. Force-distance curves were randomly obtained from 7-10 locations with 3 force curves obtained per location per sample. Force curves were analyzed using the Hertz model for spherical indenters using a custom MATLAB code [43]. Curve fits were performed for at least 1 μm of indentation depth for the samples.

2.15 Statistical analysis.

Individual sample sizes are specified in each figure caption. Comparisons between groups were assessed by unpaired *t*-test, one-way or two-way analysis of variance (ANOVA) with Tukey's multiple comparisons *post hoc* tests, as appropriate. The significance level was set at $p<0.05$ or lower. GraphPad Prism software v9.2 (GraphPad Software, La Jolla, CA, USA) was used for all analyses.

3. Results

3.1 TGFβ2 and YAP/TAZ activity is upregulated in GTM cells

It has been shown that levels of TGFβ2 are elevated in the aqueous humor of glaucomatous patients compared to age-matched normal eyes [34, 35, 44, 45]. We confirmed that GTM cells

isolated from donor eyes with POAG history secreted significantly more active TGFβ2 protein by ~2.44-fold (**Fig. 1A**) compared to normal HTM cells, which was corroborated by increased mRNA levels (**Suppl. Fig. 2**).

To investigate YAP and TAZ transcriptional activity under normal and glaucomatous conditions, the expression of YAP/TAZ and relevant select downstream targets at mRNA and protein levels were evaluated in normal HTM and GTM cells, which were plated with similar cell density. The functions of YAP/TAZ depend on their spatial localization within the cellular nucleus or cytoplasm [46]. When localized to the nucleus, YAP/TAZ interact with TEAD transcription factors to drive the expression of certain proteins, such as transglutaminase-2 (TGM2) and connective tissue growth factor (CTGF), shown to play a role in HTM cell pathobiology in glaucoma [47, 48]. When localized in the cytoplasm, YAP/TAZ can be phosphorylated by the large tumor suppressor (LATS) 1/2 kinase; phosphorylated YAP/TAZ can bind to 14-3-3σ for ubiquitin-dependent degradation [18]. We demonstrated that mRNA levels of YAP, TAZ, TGM2 and CTGF were all significantly upregulated in GTM cells compared to normal HTM cells (**Fig. 1B**). GTM cells showed significantly lower p-YAP and p-TAZ vs. normal HTM cells, while total YAP and TAZ expression were similar to HTM cells, leading to decreased p-YAP/YAP and p-TAZ/TAZ ratios. Consistent with the ratio of phosphorylated-to-total proteins, 14-3-3σ expression in GTM cells was significantly decreased compared to normal HTM cells (**Fig. 1C,D**). Besides, GTM cells exhibited significantly increased YAP/TAZ nuclear localization, YAP/TAZ nuclear-to-cytoplasmic (N/C) ratio and TGM2 expression compared to normal HTM cells (**Fig. 1E-J; Suppl. Fig. 3**). Together, these data demonstrate that levels of active TGFβ2 as well as YAP and TAZ transcriptional activity are elevated in GTM cells isolated from patients with glaucoma compared to normal HTM cells.

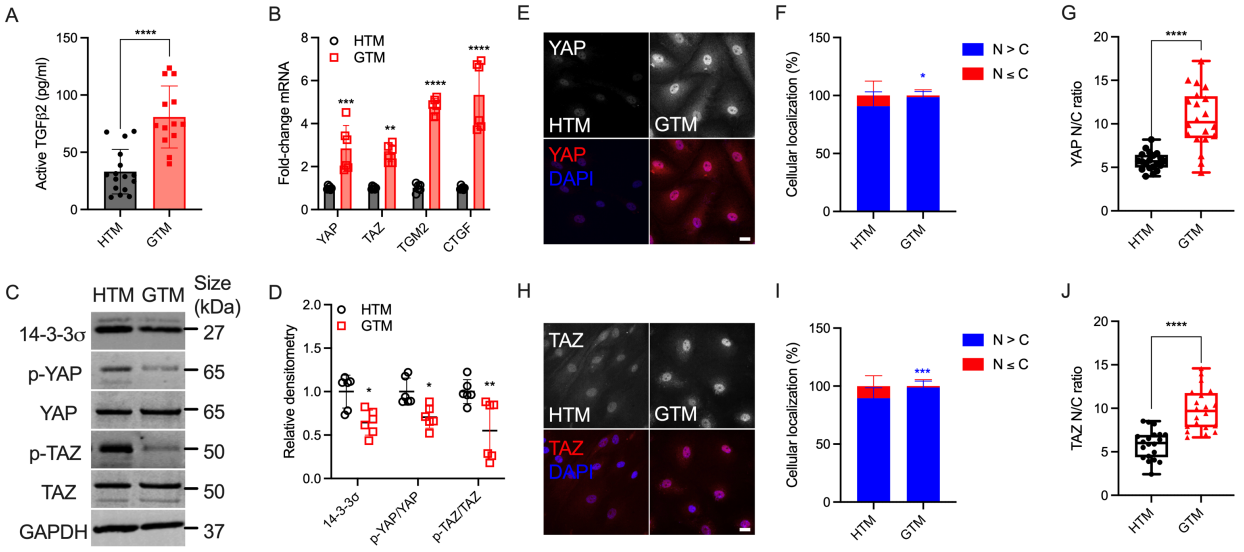

Fig. 1. Upregulated active TGFβ2 and YAP/TAZ nuclear localization in GTM cells compared to normal HTM cells. (A) Active TGFβ2 levels were quantified by ELISA (N = 16 biological replicates from 3 HTM cell strains, N = 13 biological replicates from 2 GTM cell strains). (B) mRNA fold-change of YAP, TAZ, TGM2 and CTGF by qRT-PCR (N = 6 biological replicates from 2 HTM/GTM cell strains). (C) Immunoblot of 14-3-3σ, p-YAP, p-TAZ, total YAP and total TAZ. (D) Immunoblot analysis of 14-3-3σ, p-YAP/YAP and p-TAZ/TAZ (N = 6 biological replicates from 2 HTM/GTM cell strains). (E and H) Representative fluorescence micrographs of YAP/TAZ in HTM and GTM cells (YAP/TAZ = grey or red; DAPI = blue). Scale bar, 20 μm. (F and I) Analysis of YAP/TAZ cellular localization (N > C indicates nuclear localization, N ≤ C indicates cytoplasmic localization; N = 20 images from 2 HTM/GTM cell strains with 3 biological replicates per cell strain). (G and J) Analysis of YAP/TAZ nuclear/cytoplasmic ratio (N = 20 images from 2 HTM/GTM cell strains with 3 biological replicates per cell strain). In A, B, D, F and I, the bars or lines and error bars indicate Mean ± SD; In G and J, the box and whisker plots represent median values (horizontal bars), 25th to 75th percentiles (box edges) and minimum to maximum values (whiskers), with all points plotted. Significance was determined by unpaired t-test (A, G and J) and two-way ANOVA using multiple comparisons tests (B, D, F and I) (*$p < 0.05$; **$p < 0.01$; ***$p < 0.001$; ****$p < 0.0001$).

3.2 ECM stiffening increases YAP/TAZ activity in HTM cells via modulating focal adhesions and cytoskeletal rearrangement

The TM from POAG eyes is stiffer than that from healthy eyes [29-31]. To that end, we recently showed that dexamethasone treated HTM cell-laden hydrogels are ~2-fold stiffer compared to controls [17]. Here, we demonstrated that TGFβ2-treated HTM cell encapsulated

hydrogels were also ~2-fold stiffer compared to controls using AFM and rheology (**Fig. 2A, Suppl. Fig. 4**). To mimic the stiffness difference between glaucomatous and healthy HTM tissue, we utilized riboflavin (RF)-mediated secondary UV crosslinking of collagen fibrils, which stiffened the hydrogels by ~2-fold (**Fig. 2B**).

Adherent cells are connected to the ECM through the transmembrane receptor integrins and focal adhesion (FA) proteins such as vinculin [49]. HTM cells on stiff glass were spread out with strong vinculin FA staining, while cells on soft hydrogels showed a smaller number of vinculin puncta compared to cells on glass, which was potentiated by the stiffened ECM hydrogels (**Fig. 2C,D; Suppl. 5A**). Consistent with our observation on vinculin FA, HTM cells on glass and stiff hydrogels exhibited bigger nuclei compared to cells on the soft hydrogels (glass: ~1.56-fold; stiff hydrogels: ~1.26-fold) (**Suppl. Fig. 5B**). We also found that the stiffened ECM hydrogels significantly increased filamentous (F)-actin, phospho-myosin light chain (p-MLC) and α-smooth muscle actin (αSMA) levels in HTM cells compared to cells on the soft matrix (**Fig. 2E-G, Suppl. 5C,D**). Importantly, we observed that nuclear localization of YAP/TAZ, YAP/TAZ N/C ratio, TGM2 expression, and fibronectin (FN) remodeling in HTM cells were upregulated by the stiffened ECM hydrogels compared to cells on the soft hydrogels (**Fig. 2H-M; Suppl. Fig. 5E-H**).

Together, these results suggest that the stiffened ECM hydrogels induce a more spread out HTM cell morphology compared to cells on soft matrix. The stiffened hydrogels induce cellular FA and cytoskeletal rearrangement, correlating with elevated YAP/TAZ transcriptional activity in HTM cells.

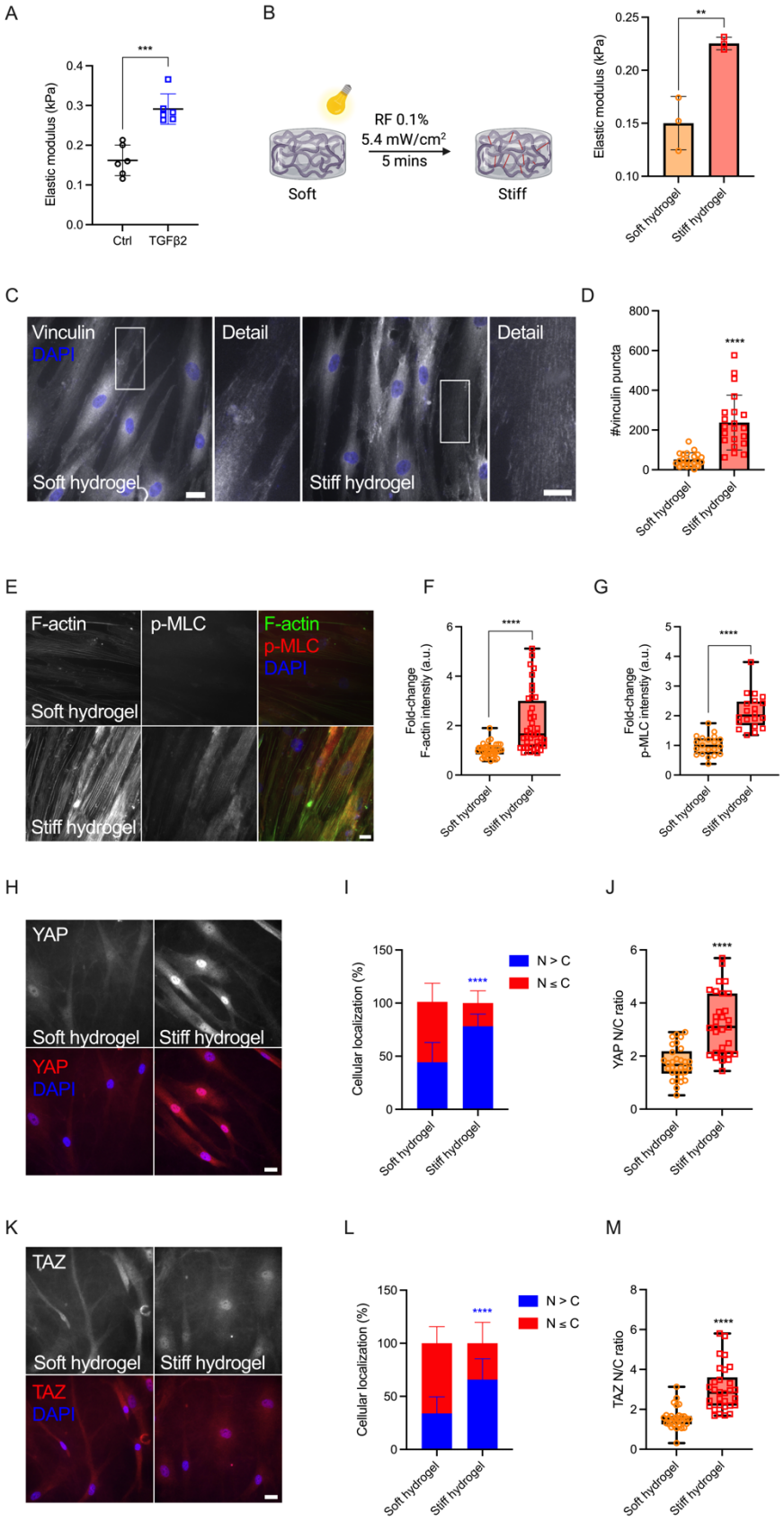

Fig. 2. Stiffened ECM hydrogels elevate YAP/TAZ activity in HTM cells via modulating FA and cytoskeletal rearrangement. (A) Elastic modulus of HTM cell-encapsulated hydrogels subjected to control and TGFβ2 (2.5 ng/mL) measured by AFM (N = 6/group). (B) Schematic of riboflavin (RF)-mediated double photo-crosslinking to stiffen ECM hydrogels, and elastic modulus of the hydrogels (N = 3/group). (C) Representative fluorescence micrographs of vinculin in HTM cells on soft and stiff hydrogels (vinculin = grey; DAPI = blue). Scale bar, 20 μm and 10 μm. (D) Analysis of vinculin puncta/image (N = 20 images from 2 HTM cell strains with 3 biological replicates per cell strain). (E) Representative fluorescence micrographs of F-actin and p-MLC in HTM cells on soft and stiff hydrogels (F-actin = green; p-MLC =red; DAPI = blue). Scale bar, 20 μm. (F and G) Quantification of F-actin and p-MLC intensity (N = 20 images per group from 2 HTM cell strains with 3 biological replicates per HTM cell strain). (H and K) Representative fluorescence micrographs of YAP/TAZ in HTM cells on soft and stiff hydrogels (YAP/TAZ = grey or red; DAPI = blue). Scale bar, 20 μm. (I and L) Analysis of YAP/TAZ cellular localization (N > C indicates nuclear localization, N ≤ C indicates cytoplasmic localization; N = 30 images from 2 HTM cell strains with 3-6 biological replicates per cell strain). (J and M) Analysis of YAP/TAZ nuclear/cytoplasmic ratio (N = 30 images from 2 HTM cell strains with 3-6 biological replicates per cell strain). In A, B, D, I and L, the bars and error bars indicate Mean ± SD; In F, G, J and M, the box and whisker plots represent median values (horizontal bars), 25th to 75th percentiles (box edges) and minimum to maximum values (whiskers), with all points plotted. Significance was determined by unpaired t-test (A, B, D, F, G, J and M) and two-way ANOVA using multiple comparisons tests (I and L) (*$p < 0.05$; **$p < 0.01$; ***$p < 0.001$; ****$p < 0.0001$).

3.3 TGFβ2 regulates YAP/TAZ activity via ERK and ROCK signaling pathways

TGFβ2 has been shown to activate canonical Smad (Smad2/3) and diverse non-Smad signaling pathways including extracellular-signal-regulated kinase (ERK), c-Jun N-terminal kinases, P38 kinases and Rho-associated kinase (ROCK) [50-53]. We recently demonstrated that TGFβ2 increased HTM cell contractility via ERK and ROCK signaling pathways by differentially regulating F-actin, αSMA, FN, and p-MLC in HTM cells [28]. Here, we investigated whether YAP signaling in HTM cells in response to TGFβ2 induction requires ERK or ROCK. HTM or GTM cells were seeded on top of soft hydrogels treated with TGFβ2 ± U0126 (ERK inhibitor) or Y27632 (ROCK inhibitor). Consistent with our observation for cells seeded on glass (**Fig. 1**), we observed significantly higher nuclear YAP/TAZ and TGM2 expression in GTM cells compared to normal HTM cells on the soft ECM hydrogels (**Fig. 3; Suppl. Fig. 6**). TGFβ2 increased nuclear YAP localization and YAP N/C ratio in both HTM and GTM cells, which were blocked by co-treatment

of U0126 or Y27632 with TGFβ2. Importantly, we observed that ROCK inhibition exhibited stronger effects on YAP nuclear localization compared to ERK inhibition (**Fig. 3A-F**).

YAP and TAZ are generally thought to have similar function in response to mechanical and biochemical signals [54]. However, it has been shown that YAP and TAZ are distinct effectors of TGFβ1-induced myofibroblast transformation [55]. In this study, we observed that TGFβ2 significantly increased nuclear TAZ in both HTM and GTM cells, and co-treatment of U0126 or Y27632 with TGFβ2 rescued TAZ nuclear localization to control levels. Surprisingly, we observed that ERK inhibition showed stronger effects on TAZ nuclear localization compared to ROCK inhibition (**Fig. 3G-L**). Consistent with YAP/TAZ nuclear localization and N/C ratio, TGM2 expression was upregulated by TGFβ2, which was significantly decreased by co-treatment of U0126 or Y27632 (**Suppl. Fig. 6**).

These data show that TGFβ2 increases nuclear YAP/TAZ and TGM2 expression in both HTM and GTM cells, which was attenuated by either U0126 or Y27632 co-treatment to varying degrees. ROCK inhibition may have a stronger effect on decreasing TGFβ2-induced YAP nuclear localization compared to ERK inhibition, whereas ERK inhibition may reduce TGFβ2-induced TAZ nuclear localization more potently than ROCK inhibition. Collectively, this suggests that external biophysical (stiffened ECM) and biochemical signals (increased TGFβ2) drive altered YAP and TAZ mechanotransduction in HTM cells that contributes to glaucomatous cellular dysfunction.

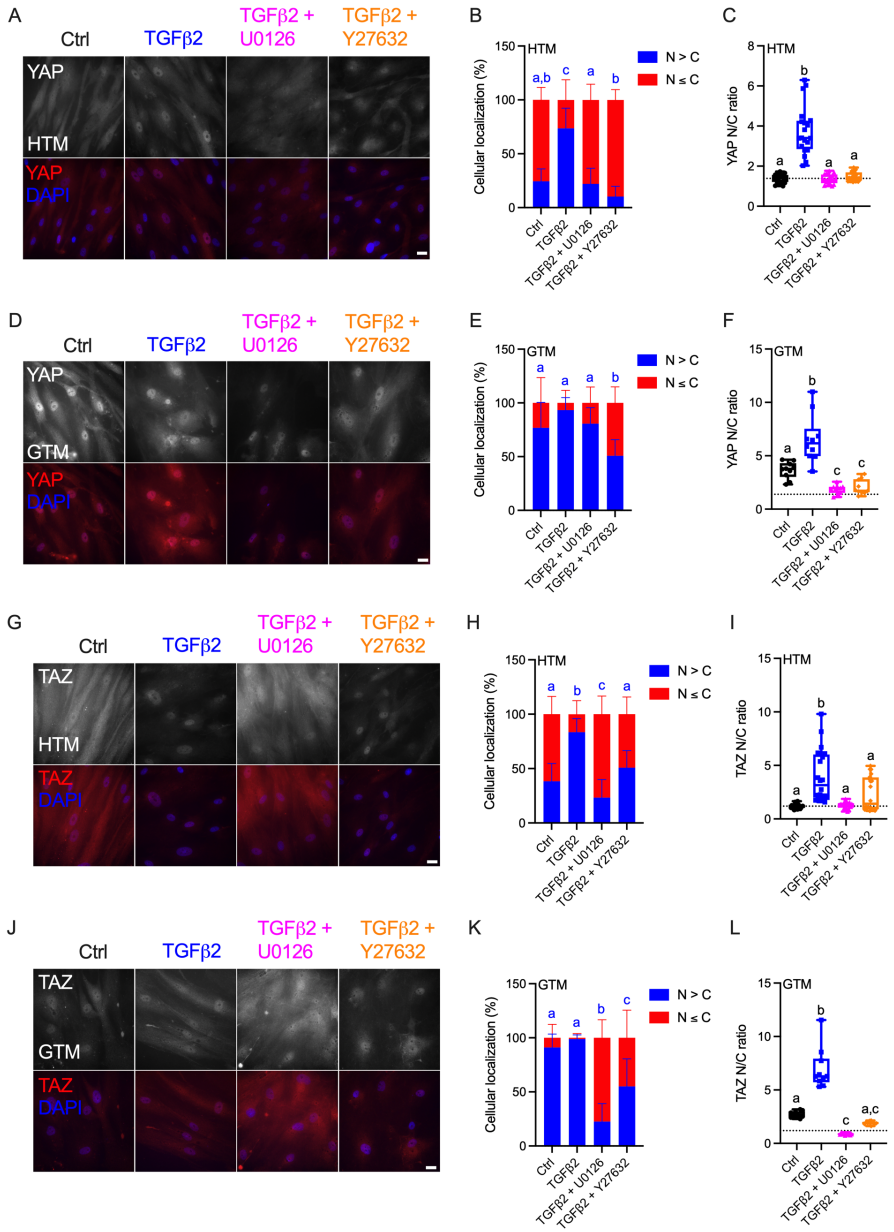

Fig. 3. Effects of TGFβ2 in absence or presence of ERK or ROCK inhibition on nuclear YAP/TAZ localization in HTM and GTM cells. (A, D, G and J) Representative fluorescence micrographs of YAP or TAZ in HTM or GTM cells on soft hydrogels subjected to control, TGFβ2 (2.5 ng/mL), TGFβ2 + U0126 (10 μM), TGFβ2 + Y27632 (10 μM) at 3 d (YAP = grey or red; DAPI = blue). Scale bar, 20 μm. (B, E, H and K) Analysis of YAP or TAZ cellular localization (N > C indicates nuclear localization, N ≤ C indicates cytoplasmic localization; N = 20 images from 2 HTM cell strains with 3 biological replicates per cell strain; N = 10 images from one GTM cell strain with 3 biological replicates). (C, F, I and L) Analysis of YAP or TAZ nuclear/cytoplasmic ratio (N = 20 images from 2 HTM cell strains with 3 biological replicates per cell strain; N = 10 images from one GTM cell strain with 3 biological replicates). In B, E, H and K the bars and error bars indicate Mean ± SD; In C, F, I and L, the box and whisker plots represent median values

(horizontal bars), 25th to 75th percentiles (box edges) and minimum to maximum values (whiskers), with all points plotted. Significance was determined by one-way (C, F, I and L) or two-way ANOVA using multiple comparisons tests (B, E, H and K) (shared significance indicator letters represent non-significant difference ($p>0.05$), distinct letters represent significant difference ($p<0.05$)).

3.4 F-actin polymerization modulates YAP/TAZ activity

It has been shown that Latrunculin B (Lat B), a compound that inhibits polymerization of the actin cytoskeleton, can increase outflow facility and decrease IOP in human and non-human primate eyes [56-58]. Likewise, Lat B has been reported to depolymerize HTM cell actin and decrease HTM cell stiffness via cell relaxation [15]. To investigate the effects of F-actin cytoskeletal disruption on YAP/TAZ activity, HTM cells were seeded on top of soft hydrogels, and treated with TGFβ2 for 3 d, followed by Lat B treatment for 30 mins (**Fig. 4A**). We observed significantly more vinculin puncta induced by TGFβ2, which was abolished by Lat B treatment (**Fig. 4B,C**). Similar to before (**Fig. 3**), TGFβ2 significantly increased YAP/TAZ nuclear localization, YAP/TAZ N/C ratio and TGM2 expression, which were restored to control levels by 30 mins of Lat B co-treatment (**Fig. 4E-L**). Immunoblot analyses corroborated the immunostaining results and showed that co-treatment of TGFβ2 and Lat B increased the ratio of p-YAP to YAP and p-TAZ to TAZ, representing overall decreased nuclear YAP and TAZ. Interestingly, according to the immunoblot result, Lat B may regulate YAP activity by increasing p-YAP while maintaining similar levels of total YAP, whereas Lat B may decrease total levels of TAZ while maintaining similar levels of p-TAZ (**Fig. 4D**).

In sum, these findings demonstrate that F-actin depolymerization decreases vinculin FA, nuclear YAP/TAZ and their downstream target TGM2.

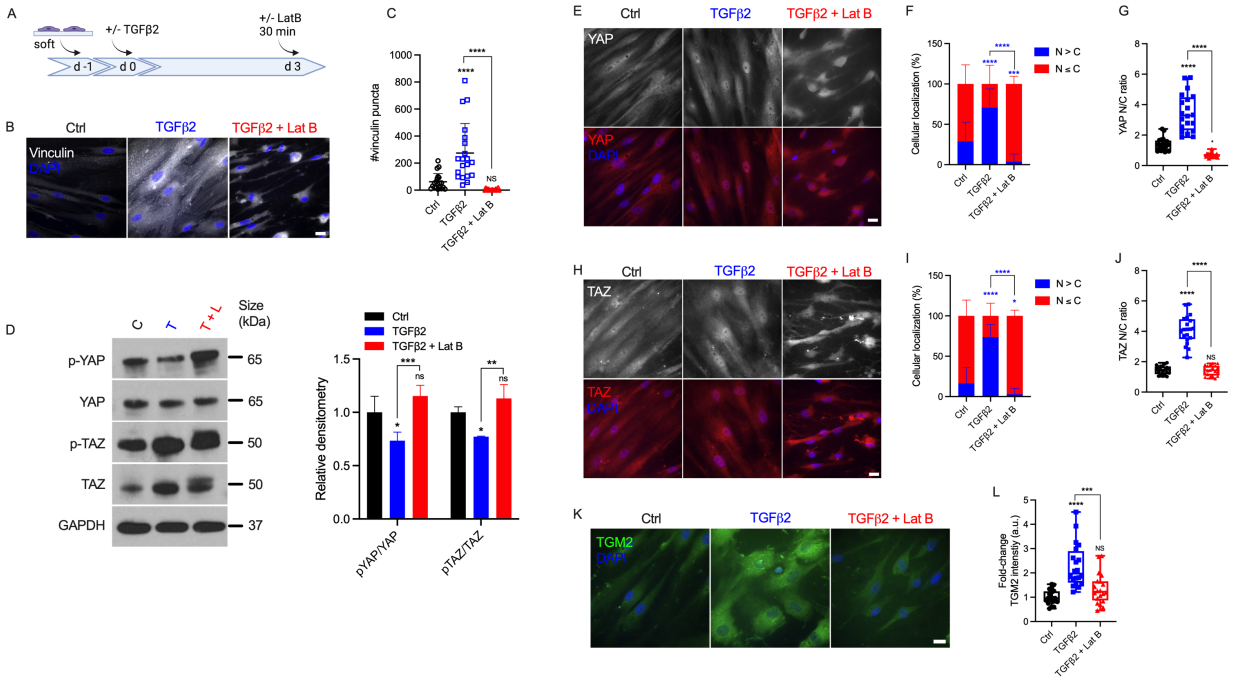

Fig. 4. Lat B reduces YAP/TAZ activity in HTM cells. (A) Schematic showing time course of Lat B experiments with HTM cells. (B) Representative fluorescence micrographs of vinculin in HTM cells on soft hydrogels subjected to control, TGFβ2 (2.5 ng/mL), TGFβ2 + Lat B (2 μM) at 3 d (vinculin = grey; DAPI = blue). Scale bar, 20 μm. (C) Analysis of number of vinculin puncta/image (N = 20 images from 2 HTM cell strains with 3 biological replicates per cell strain). (D) Immunoblot of p-YAP, total YAP, p-TAZ and total TAZ, and immunoblot analysis of p-YAP/YAP and pTAZ/TAZ (N = 3 biological replicates from one HTM cell strain). (E and H) Representative fluorescence micrographs of YAP/TAZ in HTM cells on soft hydrogels subjected to the different treatments (YAP/TAZ = grey or red; DAPI = blue). Scale bar, 20 μm. (F and I) Analysis of YAP/TAZ cellular localization (N > C indicates nuclear localization, N ≤ C indicates cytoplasmic localization; N = 20 images from 2 HTM cell strains with 3 biological replicates per cell strain). (G and J) Analysis of YAP/TAZ nuclear/cytoplasmic ratio (N = 20 images from 2 HTM cell strains with 3 biological replicates per cell strain). (K) Representative fluorescence micrographs of TGM2 in HTM cells on soft hydrogels subjected to the different treatments (TGM2 = green; DAPI = blue). Scale bar, 20 μm. (L) Analysis of TGM2 intensity (N = 20 images per group from 2 HTM cell strains with 3 biological replicates per HTM cell strain). In C, D, F, I, the bars and error bars indicate Mean ± SD; In G, J and L, the box and whisker plots represent median values (horizontal bars), 25th to 75th percentiles (box edges) and minimum to maximum values (whiskers), with all points plotted. Significance was determined by one-way (C, G, J and L) and two-way ANOVA (D, F and I) using multiple comparisons tests (*$p < 0.05$; **$p < 0.01$; ***$p < 0.001$; ****$p < 0.0001$).

3.5 YAP and TAZ regulate FA formation, ECM remodeling and cell contractile properties

Our results so far suggest that POAG-related stimuli (i.e., TGFβ2 and stiffened ECM) increase YAP/TAZ activity in HTM cells. To further investigate the roles of YAP/TAZ in HTM cell function, we seeded HTM cells on stiff hydrogels to increase the baseline levels of YAP/TAZ in controls, and depleted YAP and TAZ using combined siRNA knockdown (**Fig. 5A**). This reduced their mRNA expression levels to 34.52% and 35.25% of siRNA controls, respectively (**Fig. 5B**). The immunofluorescence results showed that both YAP/TAZ nuclear localization and N/C ratio in HTM cells transfected with siYAP/TAZ were significantly decreased vs. controls (**Fig. 5C-H**). Importantly, we observed that YAP/TAZ depletion significantly reduced expression of TGM2, FN and CTGF, which may decrease HTM ECM stiffness (**Fig. 5I-L,T**).

F-actin filaments, αSMA and p-MLC are all involved in cell contractility regulation, and we have previously demonstrated that their expression was upregulated in HTM cells under simulated glaucomatous conditions [17, 28]. Here, YAP/TAZ depletion significantly decreased F-actin filaments and expression of αSMA and p-MLC, suggestive of reduced HTM cell contractility (**Fig. 5M-Q,T**). We also found that the expression of canonical Hippo pathway kinases LATS1, LATS2 and 14-3-3σ was not affected by siYAP/TAZ knockdown (**Fig. 5V**). Tension generated within the actomyosin cytoskeleton is transmitted across FA to induce integrin-mediated remodeling of the ECM [59]. We observed that YAP/TAZ depletion significantly decreased the number of vinculin puncta and reduced nuclei size (**Fig. 5R,S,U**).

To validate the effects of siRNA-mediated YAP/TAZ depletion on HTM cell behavior under simulated glaucomatous conditions, we turned to verteporfin (VP), a selective inhibitor of the YAP/TAZ-TEAD transcriptional complex [60]. Treating HTM cells with VP significantly decreased TGFβ2-induced nuclear YAP/TAZ as well as downstream TGM2 compared to controls, consistent with the effects of siRNA-mediated YAP/TAZ depletion. We observed that the

inhibition of YAP/TAZ-TEAD interaction not only decreased nuclear YAP/TAZ, but also reduced cytoplasmic and total protein levels (**Suppl. Fig. 7**). VP treatment significantly decreased TGFβ2-induced vinculin FA formation, F-actin filaments, expression of FN, αSMA and p-MLC (**Suppl. Fig. 8**).

Collectively, these data demonstrate that YAP/TAZ depletion using siRNA or inhibition of YAP/TAZ-TEAD interaction using pharmacological inhibition leads to impaired FA formation, ECM remodeling, and cell contractile properties.

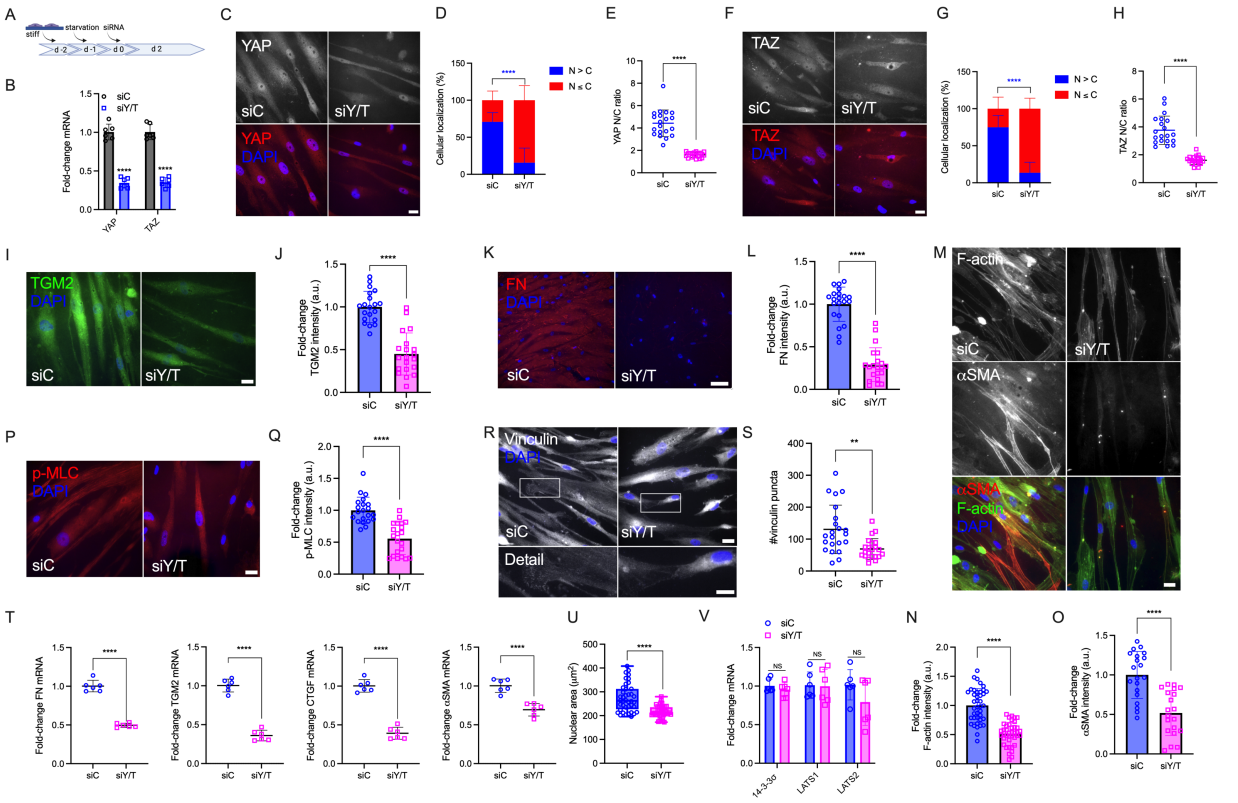

Fig. 5. YAP/TAZ are regulators of FA formation, ECM remodeling and cell contractile properties in HTM cells. (A) Schematic showing time course of YAP/TAZ depletion using siRNA experiments with HTM cells. (B) mRNA fold-change of YAP and TAZ in HTM cells on stiff hydrogels subjected to siControl or siYAP/TAZ knockdown by qRT-PCR. The mRNA levels were normalized to the levels of GAPDH mRNA 48h post transfection (N = 6 biological replicates from 2 HTM cell strain). (C and F) Representative fluorescence micrographs of YAP/TAZ in HTM cells on stiff hydrogels subjected to siControl or siYAP/TAZ (YAP/TAZ = grey or red; DAPI = blue). Scale bar, 20 μm. (D and G) Analysis of YAP/TAZ cellular localization (N > C indicates nuclear localization, N ≤ C indicates cytoplasmic localization; N = 20 images from 2 HTM cell

strains with 3 biological replicates per cell strain). (E and H) Analysis of YAP/TAZ nuclear/cytoplasmic ratio (N = 20 images from 2 HTM cell strains with 3 biological replicates per cell strain). (I, K, M, P and R) Representative fluorescence micrographs of TGM2, FN, αSMA, F-actin, p-MLC and vinculin in HTM cells on stiff hydrogels subjected to siControl or siYAP/TAZ (TGM2 = green; FN/p-MLC = red; αSMA = grey or red; F-actin = grey or green; vinculin = grey; DAPI = blue). Scale bar, 20 μm in I, M, P; 20 μm and 10 μm in R; 100 μm in K. (J, L, N, O, Q and S) Analysis of TGM2, FN, αSMA, F-actin, p-MLC and number of vinculin puncta/image (N = 20 images from 2 HTM cell strains with 3 biological replicates per cell strain). (T and V) mRNA fold-change of FN, TGM2, CTGF, αSMA, LATS1/2 and 14-3-3σ in HTM cells on stiff hydrogels subjected to siControl or siYAP/TAZ by qRT-PCR. The mRNA levels were normalized to the levels of GAPDH mRNA 48h post transfection (N = 6 biological replicates from 2 HTM cell strain). (U) Nuclear area of HTM cells on stiff hydrogels subjected to siControl or siYAP/TAZ (N = 40 images from 2 HTM cell strains with 3-6 biological replicates per cell strain; more than 100 nuclei were analyzed per cell strain). The bars and error bars indicate Mean ± SD; Significance was determined by unpaired t-test (E, H, J, L, N, O, Q, S, T and U) and two-way ANOVA (B, D, G and V) using multiple comparisons tests (*$p < 0.05$; **$p < 0.01$; ***$p < 0.001$; ****$p < 0.0001$).

3.6 YAP and TAZ mediate HTM cell contractility and HTM hydrogel stiffness

Lastly, to investigate the effects of YAP/TAZ on HTM cell contractility and ECM stiffening, we encapsulated HTM cells in ECM hydrogels and treated with TGFβ2, either alone or in combination with simvastatin or VP, and assessed hydrogel contractility and stiffness. Statins, commonly used cholesterol-lowering drugs, have been shown to exhibit ROCK inhibitory activity upstream of YAP/TAZ. Further, in a library screen of >600 FDA-approved compounds, statins were found to elicit the strongest YAP/TAZ inhibitory effect in various cancer cell lines [61-63].

TGFβ2-treated HTM hydrogels exhibited significantly greater contraction vs. controls by 5 d (74.30% of controls), consistent with our previous report [17]. Co-treatment of TGFβ2 + simvastatin or VP potently decreased HTM hydrogel contraction (95.28% of controls and 90.37% of controls, respectively) compared to TGFβ2-treated samples (**Fig. 6A**). We observed that TGFβ2 significantly increased hydrogel stiffness (1.60-fold of controls), which was prevented by co-treatment with simvastatin (0.59-fold of controls) or VP (1.05-fold of controls) (**Fig. 6B**).

To assess whether YAP/TAZ inhibition had comparable effects on GTM cells, we evaluated GTM cell-laden hydrogel contraction in response to the same treatments. Our results demonstrated that GTM hydrogels in absence of additional TGFβ2 induction exhibited significantly greater contraction relative to normal HTM hydrogels (86.08% of HTM hydrogels controls); TGFβ2 further increased GTM hydrogel contraction, and both simvastatin and VP partially blocked this during the short 5 d exposure (**Fig. 6C**).

To determine if hydrogel contractility was influenced by the cell number, we assessed HTM/GTM cell proliferation in constructs subjected to the different treatments. We observed a smaller number of cells in the TGFβ2 + VP group compared to TGFβ2-treated samples (10.10% decreased) (**Suppl. Fig. 9A**), while co-treatment of TGFβ2 + VP reduced hydrogel contraction and stiffening by 21.63% and 51.62% compared to the TGFβ2-treated group, respectively (**Fig. 6A,B**). No significant differences between the different groups were observed for GTM cell-laden hydrogels (**Suppl. Fig. 9B**).

Together, these data demonstrate that TGFβ2 robustly induces HTM hydrogel contractility and stiffening in a soft ECM environment, which are potently reduced by YAP/TAZ inhibition. Likewise, inhibition of YAP/TAZ had similar effects on GTM cells inside the 3D hydrogel network, albeit at overall reduced levels compared to induced normal HTM cells, possibly related to their inherent pathological cellular phenotype.

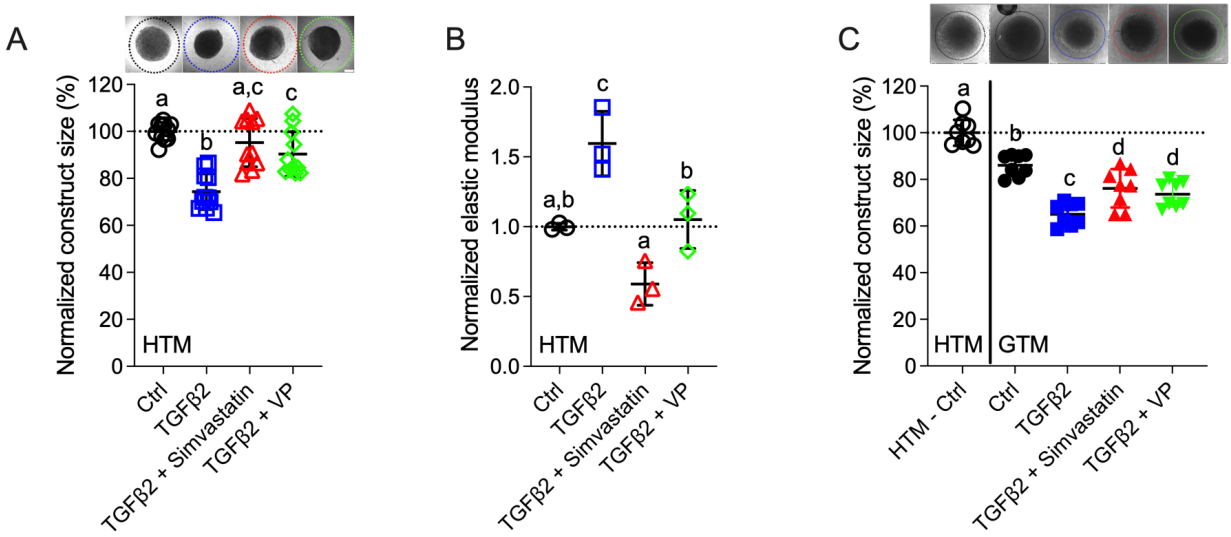

Fig. 6. Inhibition of YAP/TAZ activity decreases HTM hydrogel contractility and stiffness. (A) Representative brightfield images and construct size quantification of HTM hydrogels subjected to control, TGFβ2 (2.5 ng/ml), TGFβ2 + simvastatin (10 µM), TGFβ2 + VP (0.5 µM) at 5 d. (dashed lines outline original size of constructs at 0 d. Scale bar, 1 mm; N = 11 hydrogels per group from 2 HTM cell strains). (B) Normalized elastic modulus (to controls) of HTM hydrogels subjected to the different treatments at 5 d (N=3 per group). (C) Representative brightfield images and construct size quantification of HTM hydrogels control and GTM hydrogels subjected to the different treatments at 5 d (dashed lines outline original size of constructs at 0 d. Scale bar, 1 mm; N = 8 hydrogels per group from 2 HTM/GTM cell strains). The bars and error bars indicate Mean ± SD; dotted line shows control value for reference; Significance was determined by one-way ANOVA using multiple comparisons tests (shared significance indicator letters represent non-significant difference ($p>0.05$), distinct letters represent significant difference ($p<0.05$)).

4. Discussion

The mechanosensitive transcription factors YAP and TAZ play important roles in mechanotransduction, a process through which cells translate external biophysical cues into internal biochemical signals. YAP/TAZ modulate target gene expression profiles with broad functional consequences across many cell and tissue types [18, 19]. Through this mechanism, YAP/TAZ signaling regulates critical cellular functions and normal tissue homeostasis; imbalance or failure of this process is at the core of various diseases [64]. Indeed, elevated YAP/TAZ transcriptional activity is associated with glaucomatous HTM cell dysfunction [20, 21, 24, 65-68]. YAP/TAZ activity is upregulated in GTM cells from patients with glaucoma compared to HTM

cells isolated from normal HTM tissues (**Fig. 1**). However, the detailed mechanisms for YAP/TAZ modulation in HTM cells under glaucomatous conditions (i.e., stiffened ECM and increased growth factors in AH) remain to be elucidated. Here, we used biomimetic ECM hydrogels with tunable stiffness to study the roles of YAP and TAZ in HTM cells in response to stiffened matrix and TGFβ2. As summarized in **Fig. 7**, our data support that YAP/TAZ are critical regulators in mediating cellular responses to the stiffened ECM and elevated TGFβ2 in POAG; we propose that increased YAP/TAZ activity may drive further HTM tissue stiffening to exacerbate disease pathology conditions. This conclusion is supported by the findings that (i) stiffened ECM hydrogels elevate YAP/TAZ activity, as indicated by nuclear localization of YAP/TAZ, potentially through regulating focal adhesion (FA) formation and cytoskeleton rearrangement; (ii) TGFβ2 induces nuclear YAP/TAZ localization and target gene activation to varying degrees through ERK and ROCK signaling pathways; (iii) depolymerization of F-actin decreases YAP/TAZ activity; (iv) YAP/TAZ depletion using siRNA or pharmacological inhibition of YAP/TAZ-TEAD interaction decreases FA formation, ECM remodeling and cell contractile properties; (v) YAP/TAZ inhibitors VP and simvastatin decrease HTM cell-laden hydrogel contraction and stiffening.

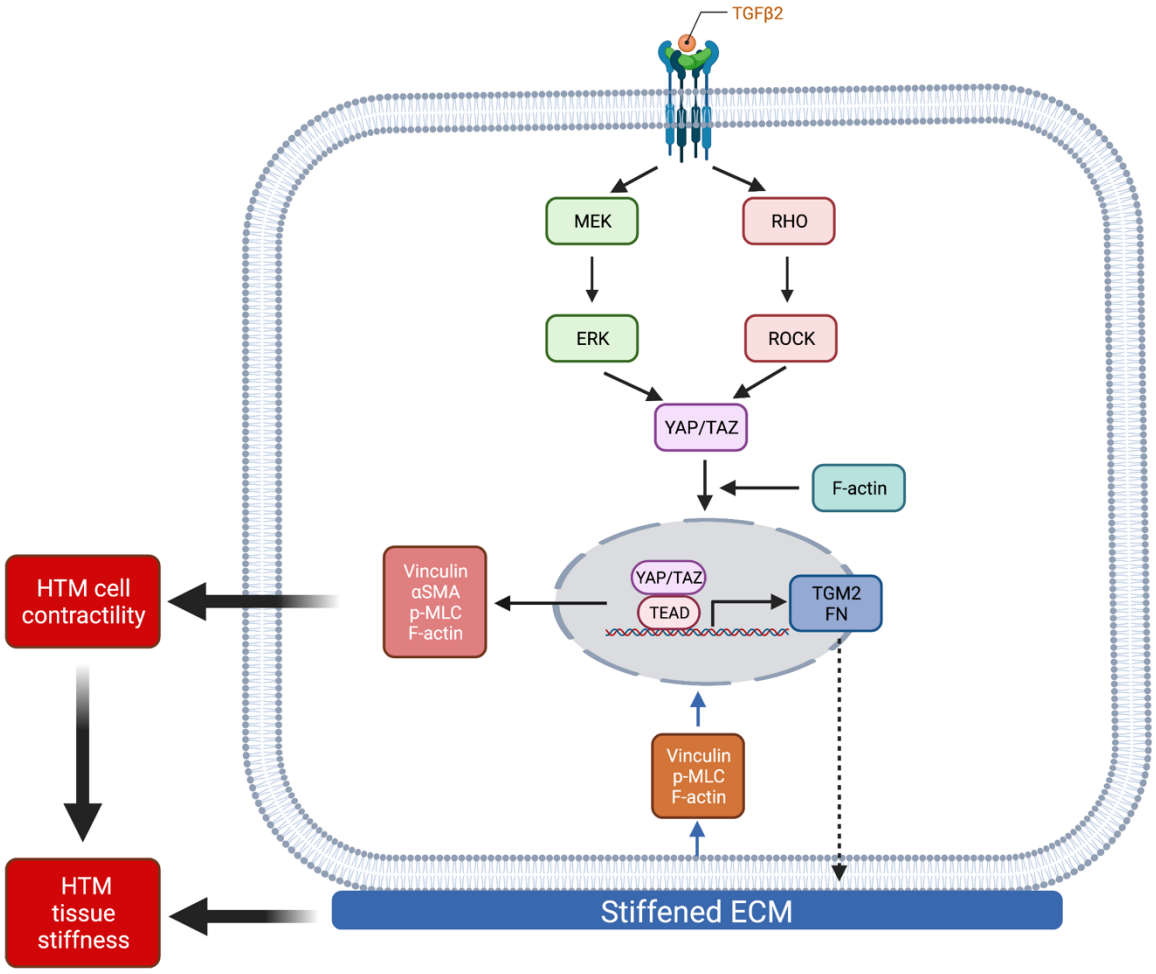

Fig. 7. Schematic illustration of the effects elicited by ECM stiffness and TGFβ2 that modulate YAP/TAZ activity in HTM cells. Stiffened ECM hydrogels elevate YAP/TAZ activity potentially through regulating focal adhesion (FA) formation and cytoskeleton rearrangement. TGFβ2 activates ERK and ROCK signaling pathways to regulate YAP/TAZ activity in normal HTM and GTM cells. YAP/TAZ activation induces HTM cell contractility and ECM remodeling, which together may increase HTM stiffness in POAG. Created with BioRender.com.

Most *in vitro* studies of HTM cell (patho-)physiology have relied on conventional cell monolayer cultures on plastic or glass of supraphysiologic stiffness. However, biophysical cues such as substrate composition and stiffness are known to be potent modulators of cell behaviors [23]. Increased tissue stiffness has been observed in multiple pathologies, including cancer, cardiovascular and fibrosis-related diseases [13]. ECM stiffening can precede disease development

and consequently increased mechanical cues can drive their progression via altered mechanotransduction [12, 69, 70]. Therefore, therapeutically targeting ECM stiffening by disrupting the cellular response to the stiffened ECM environment, or in other words targeting mechanotransduction, is an emerging field with clear implications for glaucoma treatment. It is widely accepted that the ECM is stiffer in the glaucomatous HTM [71]. Previous studies have also shown that ECM deposited by HTM cells treated with DEX was ~2-4-fold stiffer relative to controls [42, 72]. Our recent data using DEX-induced HTM cell-encapsulated 3D ECM hydrogels were in good agreement with these observations [17]. In this study, we demonstrated that TGFβ2 treatment resulted in a comparable ~2-fold increase in ECM stiffness surrounding the HTM cells as they reside embedded in our bioengineered hydrogels. In both scenarios, the stiffness changes were cell-driven in response to biochemical cues implicated in glaucoma.

Corneal UV crosslinking with riboflavin (RF) is a clinical treatment to stabilize the collagen-rich stroma in corneal ectasias [73, 74], with promising potential for enhancing mechanical properties of collagen-based hydrogels [75, 76]. Crosslinking occurs via covalent bond formation between amino acids of collagen fibrils induced by singlet O_2 from UV-excited RF [77]. To simulate glaucomatous ECM stiffening for investigations of the cellular response, we used riboflavin to double-crosslink collagen in the hydrogels, which increased their stiffness ~2-fold over baseline (**Fig. 2B**). HTM cells on the stiffened hydrogels exhibited bigger nuclei, increased number of vinculin FA, cytoskeleton rearrangement and YAP/TAZ nuclear localization compared to cells on the soft hydrogels (**Fig. 2C-M**). Taken together, our findings indicate that YAP/TAZ activity in HTM cells is distinctive on the different substrates, suggesting that hydrogels with tunable physiochemical properties may be more suitable to investigate subtleties in HTM cell

behaviors that would otherwise go unnoticed when relying exclusively on traditional stiff 2D culture substrates.

It has been shown that levels of TGFβ2 are elevated in the aqueous humor of glaucomatous patients compared to age-matched normal eyes [34, 35, 44, 45]. Here, we confirmed that GTM cells isolated from POAG donor eyes secreted significantly more active TGFβ2 compared to normal HTM cells (**Fig. 1A; Suppl. Fig. 2**). We observed that TGFβ2 upregulated YAP/TAZ nuclear localization and TGM2 expression, downstream target of nuclear YAP/TAZ, in both normal HTM and GTM cells (**Fig. 3**). YAP and TAZ can have either convergent or divergent functions depending on context. Global YAP knockout mice display embryonic death caused by yolk sac vasculogenesis defects, whereas TAZ knockout mice, which have defects in kidney function, can partly reach adulthood [78-80]. In corneal fibroblasts, YAP and TAZ have different functions during TGFβ1-induced myofibroblast transformation, while YAP and TAZ show similar effects in modulating the profibrotic responses in dermal fibroblasts [55, 81]. Interestingly, we observed that ROCK inhibition had a greater effect on reducing nuclear TAZ localization, whereas ERK inhibition had a stronger influence on decreasing nuclear YAP (**Fig. 3**). Further research will be necessary to investigate in greater detail how ERK and ROCK signaling differentially regulate YAP and TAZ activity in HTM cells.

It has been demonstrated that actomyosin cell contractility forces are increased in response to elevated ECM stiffness and TGFβ2 induction [13, 28]. Additionally, we have demonstrated that the stiffened ECM matrix induced YAP/TAZ nuclear localization, and increased F-actin filaments, p-MLC and αSMA - all involved in actomyosin cell contractility force generation. We hypothesized that increased actomyosin cell contractility may drive YAP/TAZ nuclear localization in HTM cells. Here, we used Lat B to decrease F-actin stress fibers and increase cytoskeletal

relaxation. We found that a short exposure time to Lat B eliminated vinculin FA formation and YAP/TAZ nuclear localization, and decreased TGM2 expression. ROCK inhibition has also been shown to decrease HTM cell F-actin fibers and contractility [17]. These observations on effects of Lat B were consistent with our findings that ROCK inhibitor reduced YAP/TAZ activity. It would be worthwhile to further investigate effects of other cell contractility related molecules, such as myosin light chain kinase, myosin II, cofilin and gelsolin, on YAP/TAZ activity in HTM cells.

We have observed that simulated glaucomatous conditions (i.e., elevated TGFβ2 and stiffened ECM) upregulated YAP/TAZ activity, and treatments that can reduce IOP in experimental models (i.e., ROCK inhibitor and Lat B) downregulated YAP/TAZ activity. These observations led us to explore the role of YAP/TAZ on glaucoma pathology development. We found that YAP/TAZ depletion using siRNA and inhibition of YAP/TAZ-TEAD interaction using VP consistently decreased FA formation (i.e., vinculin), and reduced expression of cell contractile proteins (i.e., F-actin, p-MLC and αSMA) and ECM proteins (i.e., FN) (**Fig. 5; Suppl. Fig. 8**). Also, YAP/TAZ deactivation reduced expression of TGM2, a protein that promotes cell-matrix interactions and FN crosslinking to stiffen ECM [82], and CTGF, known to increase ECM production and cell contractility in HTM cells, and elevate IOP in mouse eyes [48]. Thus, YAP/TAZ inhibition may decrease subsequent ECM stiffness potentially through regulation of ECM, TGM2 and CTGF production. Notably, YAP/TAZ inhibition using simvastatin and VP blunted HTM cell-laden hydrogel contraction and stiffening (**Fig. 6A-C**). Thus, we conclude that YAP/TAZ act as central players in regulating HTM cell mechanical homeostasis in response to changes of the surrounding environment (e.g., levels of growth factors, ECM stiffness and composition) to maintain tissue-level structural integrity and functionality. It has been demonstrated that the relative roles of YAP/TAZ are cell type- and context-dependent; they can cause homeostatic regulation of tissue

properties (negative feedback loop) or promote fibrotic conditions (positive feedback loop). Some reports implicated YAP/TAZ in a feed-forward promotion of cytoskeletal tension and ECM proteins deposition [20, 83, 84], while some research showed YAP/TAZ had a negative feedback regulation that acted to suppress actin polymerization and cytoskeletal tension [85, 86]. Our data were consistent with the former; i.e., YAP/TAZ drives HTM cell contraction and ECM stiffening.

In conclusion, using our ECM hydrogel system, we demonstrated that YAP/TAZ activity is upregulated in response to simulated glaucomatous conditions (i.e., TGFβ2 induction and stiffened ECM), and that YAP/TAZ activation induces HTM cell contractility and ECM remodeling, which together may increase HTM stiffness in POAG. Our findings provide strong evidence for a pathologic role of aberrant YAP/TAZ signaling in glaucomatous HTM cell dysfunction, and may help inform strategies for the development of novel multifactorial approaches to prevent progressive ocular hypertension in glaucoma.

Disclosure

The authors report no conflicts of interest.

Funding

This project was supported in part by National Institutes of Health grants R01EY026048, R01EY031710, K08EY031755 (to VK.R., W.D.S., and P.S.G), an American Glaucoma Society Young Clinician Scientist Award (to P.S.G.), a Syracuse University BioInspired Pilot Grant (to S.H.), unrestricted grants to SUNY Upstate Medical University Department of Ophthalmology

and Visual Sciences from Research to Prevent Blindness (RPB) and from Lions Region 20-Y1, and RPB Career Development Awards (to P.S.G. and S.H.).

Acknowledgments

We thank Dr. Robert W. Weisenthal and the team at Specialty Surgery Center of Central New York for assistance with corneal rim specimens. We also thank Dr. Nasim Annabi at the University of California – Los Angeles for providing the KCTS-ELP, Dr. Alison Patteson at Syracuse University for rheometer access, and Drs. Audrey M. Bernstein and Mariano S. Viapiano at Upstate Medical University for imaging support. **Author contributions:** H.L., VK.R., W.D.S., P.S.G., and S.H. designed all experiments, collected, analyzed, and interpreted the data. W.D.S. provided the GTM cells. VK.R. performed the AFM experiments. H.L. and S.H. wrote the manuscript. All authors commented on and approved the final manuscript. P.S.G. and S.H. conceived and supervised the research. **Competing interests:** The authors declare no conflict of interest. **Data and materials availability:** All data needed to evaluate the conclusions in the paper are present in the paper and/or the Supplementary Materials. Additional data related to this paper may be requested from the authors.

References

1. Quigley, H.A., *Open-angle glaucoma.* N Engl J Med, 1993. **328**(15): p. 1097-106.
2. Quigley, H.A. and A.T. Broman, *The number of people with glaucoma worldwide in 2010 and 2020.* Br J Ophthalmol, 2006. **90**(3): p. 262-7.
3. Kwon, Y.H., et al., *Primary open-angle glaucoma.* N Engl J Med, 2009. **360**(11): p. 1113-24.
4. Tham, Y.C., et al., *Global prevalence of glaucoma and projections of glaucoma burden through 2040: a systematic review and meta-analysis.* Ophthalmology, 2014. **121**(11): p. 2081-90.
5. Tamm, E.R., B.M. Braunger, and R. Fuchshofer, *Intraocular Pressure and the Mechanisms Involved in Resistance of the Aqueous Humor Flow in the Trabecular Meshwork Outflow Pathways.* Prog Mol Biol Transl Sci, 2015. **134**: p. 301-14.
6. Brubaker, R.F., *Flow of aqueous humor in humans [The Friedenwald Lecture].* Invest Ophthalmol Vis Sci, 1991. **32**(13): p. 3145-66.
7. Acott, T.S. and M.J. Kelley, *Extracellular matrix in the trabecular meshwork.* Exp Eye Res, 2008. **86**(4): p. 543-61.
8. Tamm, E.R., *The trabecular meshwork outflow pathways: structural and functional aspects.* Exp Eye Res, 2009. **88**(4): p. 648-55.
9. Hann, C.R. and M.P. Fautsch, *The elastin fiber system between and adjacent to collector channels in the human juxtacanalicular tissue.* Invest Ophthalmol Vis Sci, 2011. **52**(1): p. 45-50.
10. Abu-Hassan, D.W., T.S. Acott, and M.J. Kelley, *The Trabecular Meshwork: A Basic Review of Form and Function.* J Ocul Biol, 2014. **2**(1): p. 9.
11. Keller, K.E. and T.S. Acott, *The Juxtacanalicular Region of Ocular Trabecular Meshwork: A Tissue with a Unique Extracellular Matrix and Specialized Function.* J Ocul Biol, 2013. **1**(1): p. 3.
12. Frantz, C., K.M. Stewart, and V.M. Weaver, *The extracellular matrix at a glance.* J Cell Sci, 2010. **123**(Pt 24): p. 4195-200.
13. Lampi, M.C. and C.A. Reinhart-King, *Targeting extracellular matrix stiffness to attenuate disease: From molecular mechanisms to clinical trials.* Sci Transl Med, 2018. **10**(422).
14. Han, H., et al., *Elasticity-Dependent Modulation of TGF-β Responses in Human Trabecular Meshwork Cells.* Investigative Ophthalmology & Visual Science, 2011. **52**(6): p. 2889-2896.
15. McKee, C.T., et al., *The effect of biophysical attributes of the ocular trabecular meshwork associated with glaucoma on the cell response to therapeutic agents.* Biomaterials, 2011. **32**(9): p. 2417-2423.
16. Schlunck, G.n., et al., *Substrate Rigidity Modulates Cell–Matrix Interactions and Protein Expression in Human Trabecular Meshwork Cells.* Investigative Ophthalmology & Visual Science, 2008. **49**(1): p. 262-269.
17. Li, H., et al., *A tissue-engineered human trabecular meshwork hydrogel for advanced glaucoma disease modeling.* Exp Eye Res, 2021. **205**: p. 108472.
18. Dupont, S., et al., *Role of YAP/TAZ in mechanotransduction.* Nature, 2011. **474**(7350): p. 179-183.

19. Boopathy, G.T.K. and W. Hong, *Role of Hippo Pathway-YAP/TAZ Signaling in Angiogenesis.* Frontiers in Cell and Developmental Biology, 2019. **7**(49).
20. Yemanyi, F. and V. Raghunathan, *Lysophosphatidic Acid and IL-6 Trans-signaling Interact via YAP/TAZ and STAT3 Signaling Pathways in Human Trabecular Meshwork Cells.* Invest Ophthalmol Vis Sci, 2020. **61**(13): p. 29.
21. Peng, J., et al., *YAP and TAZ mediate steroid-induced alterations in the trabecular meshwork cytoskeleton in human trabecular meshwork cells.* Int J Mol Med, 2018. **41**(1): p. 164-172.
22. Honjo, M., et al., *Role of the Autotaxin-LPA Pathway in Dexamethasone-Induced Fibrotic Responses and Extracellular Matrix Production in Human Trabecular Meshwork Cells.* Investigative Ophthalmology & Visual Science, 2018. **59**(1): p. 21-30.
23. Raghunathan, V.K., et al., *Role of substratum stiffness in modulating genes associated with extracellular matrix and mechanotransducers YAP and TAZ.* Invest Ophthalmol Vis Sci, 2013. **54**(1): p. 378-86.
24. Thomasy, S.M., et al., *Substratum stiffness and latrunculin B modulate the gene expression of the mechanotransducers YAP and TAZ in human trabecular meshwork cells.* Exp Eye Res, 2013. **113**: p. 66-73.
25. Yemanyi, F., J. Vranka, and V.K. Raghunathan, *Crosslinked Extracellular Matrix Stiffens Human Trabecular Meshwork Cells Via Dysregulating β-catenin and YAP/TAZ Signaling Pathways.* Investigative Ophthalmology & Visual Science, 2020. **61**(10): p. 41-41.
26. Drury, J.L. and D.J. Mooney, *Hydrogels for tissue engineering: scaffold design variables and applications.* Biomaterials, 2003. **24**(24): p. 4337-4351.
27. Panahi, R. and M. Baghban-Salehi, *Protein-Based Hydrogels*, in *Cellulose-Based Superabsorbent Hydrogels*, M.I.H. Mondal, Editor. 2019, Springer International Publishing: Cham. p. 1561-1600.
28. Li, H., et al., *TGFβ2 regulates human trabecular meshwork cell contractility via ERK and ROCK pathways with distinct signaling crosstalk dependent on the culture substrate.* bioRxiv, 2021: p. 2021.07.01.450718.
29. Last, J.A., et al., *Elastic Modulus Determination of Normal and Glaucomatous Human Trabecular Meshwork.* Investigative Ophthalmology & Visual Science, 2011. **52**(5): p. 2147-2152.
30. Vahabikashi, A., et al., *Increased stiffness and flow resistance of the inner wall of Schlemm's canal in glaucomatous human eyes.* Proceedings of the National Academy of Sciences, 2019. **116**(52): p. 26555-26563.
31. Wang, K., et al., *Estimating Human Trabecular Meshwork Stiffness by Numerical Modeling and Advanced OCT Imaging.* Investigative Ophthalmology & Visual Science, 2017. **58**(11): p. 4809-4817.
32. Fuchshofer, R. and E.R. Tamm, *Modulation of extracellular matrix turnover in the trabecular meshwork.* Experimental Eye Research, 2009. **88**(4): p. 683-688.
33. Granstein, R.D., et al., *Aqueous humor contains transforming growth factor-beta and a small (less than 3500 daltons) inhibitor of thymocyte proliferation.* J Immunol, 1990. **144**(8): p. 3021-7.
34. Inatani, M., et al., *Transforming growth factor-beta 2 levels in aqueous humor of glaucomatous eyes.* Graefes Arch Clin Exp Ophthalmol, 2001. **239**(2): p. 109-13.

35. Agarwal, P., A.M. Daher, and R. Agarwal, *Aqueous humor TGF-β2 levels in patients with open-angle glaucoma: A meta-analysis.* Molecular vision, 2015. **21**: p. 612-620.
36. Kasetti, R.B., et al., *Transforming growth factor β2 (TGFβ2) signaling plays a key role in glucocorticoid-induced ocular hypertension.* J Biol Chem, 2018. **293**(25): p. 9854-9868.
37. Stamer, W.D., et al., *Isolation and culture of human trabecular meshwork cells by extracellular matrix digestion.* Curr Eye Res, 1995. **14**(7): p. 611-7.
38. Keller, K.E., et al., *Consensus recommendations for trabecular meshwork cell isolation, characterization and culture.* Exp Eye Res, 2018. **171**: p. 164-173.
39. Schindelin, J., et al., *Fiji: an open-source platform for biological-image analysis.* Nat Methods, 2012. **9**(7): p. 676-82.
40. Schmittgen, T.D. and K.J. Livak, *Analyzing real-time PCR data by the comparative C(T) method.* Nature Protocols, 2008. **3**(6): p. 1101-8.
41. Timothy P. Lodge, P.C.H., *Polymer Chemistry.* CRC Press, 2020.
42. Raghunathan, V.K., et al., *Glaucomatous cell derived matrices differentially modulate non-glaucomatous trabecular meshwork cellular behavior.* Acta Biomater, 2018. **71**: p. 444-459.
43. Chang, Y.R., et al., *Automated AFM force curve analysis for determining elastic modulus of biomaterials and biological samples.* J Mech Behav Biomed Mater, 2014. **37**: p. 209-18.
44. Ochiai, Y. and H. Ochiai, *Higher concentration of transforming growth factor-beta in aqueous humor of glaucomatous eyes and diabetic eyes.* Jpn J Ophthalmol, 2002. **46**(3): p. 249-53.
45. Picht, G., et al., *Transforming growth factor beta 2 levels in the aqueous humor in different types of glaucoma and the relation to filtering bleb development.* Graefes Arch Clin Exp Ophthalmol, 2001. **239**(3): p. 199-207.
46. Low, B.C., et al., *YAP/TAZ as mechanosensors and mechanotransducers in regulating organ size and tumor growth.* FEBS Lett, 2014. **588**(16): p. 2663-70.
47. Tovar-Vidales, T., et al., *Tissue transglutaminase expression and activity in normal and glaucomatous human trabecular meshwork cells and tissues.* Investigative ophthalmology & visual science, 2008. **49**(2): p. 622-628.
48. Junglas, B., et al., *Connective Tissue Growth Factor Causes Glaucoma by Modifying the Actin Cytoskeleton of the Trabecular Meshwork.* The American Journal of Pathology, 2012. **180**(6): p. 2386-2403.
49. Mohammed, D., et al., *Innovative Tools for Mechanobiology: Unraveling Outside-In and Inside-Out Mechanotransduction.* Frontiers in Bioengineering and Biotechnology, 2019. **7**(162).
50. Zhang, Y.E., *Non-Smad pathways in TGF-β signaling.* Cell Research, 2009. **19**(1): p. 128-139.
51. Ma, J., et al., *TGF-β-Induced Endothelial to Mesenchymal Transition in Disease and Tissue Engineering.* Frontiers in cell and developmental biology, 2020. **8**: p. 260-260.
52. Prendes, M.A., et al., *The role of transforming growth factor β in glaucoma and the therapeutic implications.* Br J Ophthalmol, 2013. **97**(6): p. 680-6.
53. Montecchi-Palmer, M., et al., *TGFβ2 Induces the Formation of Cross-Linked Actin Networks (CLANs) in Human Trabecular Meshwork Cells Through the Smad and Non-*

Smad Dependent Pathways. Investigative ophthalmology & visual science, 2017. **58**(2): p. 1288-1295.

54. Totaro, A., T. Panciera, and S. Piccolo, *YAP/TAZ upstream signals and downstream responses.* Nature Cell Biology, 2018. **20**(8): p. 888-899.
55. Muppala, S., et al., *YAP and TAZ are distinct effectors of corneal myofibroblast transformation.* Exp Eye Res, 2019. **180**: p. 102-109.
56. Tian, B., et al., *Cytoskeletal Involvement in the Regulation of Aqueous Humor Outflow.* Investigative Ophthalmology & Visual Science, 2000. **41**(3): p. 619-623.
57. Peterson, J.A., et al., *Latrunculin-A increases outflow facility in the monkey.* Invest Ophthalmol Vis Sci, 1999. **40**(5): p. 931-41.
58. Ethier, C.R., A.T. Read, and D.W. Chan, *Effects of latrunculin-B on outflow facility and trabecular meshwork structure in human eyes.* Invest Ophthalmol Vis Sci, 2006. **47**(5): p. 1991-8.
59. Jansen, K.A., P. Atherton, and C. Ballestrem, *Mechanotransduction at the cell-matrix interface.* Semin Cell Dev Biol, 2017. **71**: p. 75-83.
60. Liu-Chittenden, Y., et al., *Genetic and pharmacological disruption of the TEAD-YAP complex suppresses the oncogenic activity of YAP.* Genes Dev, 2012. **26**(12): p. 1300-5.
61. Wang, C.Y., P.Y. Liu, and J.K. Liao, *Pleiotropic effects of statin therapy: molecular mechanisms and clinical results.* Trends Mol Med, 2008. **14**(1): p. 37-44.
62. Sorrentino, G., et al., *Metabolic control of YAP and TAZ by the mevalonate pathway.* Nat Cell Biol, 2014. **16**(4): p. 357-66.
63. Wang, Z., et al., *Interplay of mevalonate and Hippo pathways regulates RHAMM transcription via YAP to modulate breast cancer cell motility.* Proc Natl Acad Sci U S A, 2014. **111**(1): p. E89-98.
64. Panciera, T., et al., *Mechanobiology of YAP and TAZ in physiology and disease.* Nat Rev Mol Cell Biol, 2017. **18**(12): p. 758-770.
65. Yemanyi, F., J. Vranka, and V.K. Raghunathan, *Crosslinked Extracellular Matrix Stiffens Human Trabecular Meshwork Cells Via Dysregulating beta-catenin and YAP/TAZ Signaling Pathways.* Invest Ophthalmol Vis Sci, 2020. **61**(10): p. 41.
66. Chen, W.S., et al., *Verteporfin without light stimulation inhibits YAP activation in trabecular meshwork cells: Implications for glaucoma treatment.* Biochem Biophys Res Commun, 2015. **466**(2): p. 221-5.
67. Ho, L.T.Y., et al., *Lysophosphatidic Acid Induces ECM Production via Activation of the Mechanosensitive YAP/TAZ Transcriptional Pathway in Trabecular Meshwork Cells.* Invest Ophthalmol Vis Sci, 2018. **59**(5): p. 1969-1984.
68. Dhamodaran, K., et al., *Wnt Activation After Inhibition Restores Trabecular Meshwork Cells Toward a Normal Phenotype.* Invest Ophthalmol Vis Sci, 2020. **61**(6): p. 30.
69. Pickup, M.W., J.K. Mouw, and V.M. Weaver, *The extracellular matrix modulates the hallmarks of cancer.* EMBO Rep, 2014. **15**(12): p. 1243-53.
70. Kaess, B.M., et al., *Aortic stiffness, blood pressure progression, and incident hypertension.* Jama, 2012. **308**(9): p. 875-81.
71. Wang, K., et al., *Trabecular meshwork stiffness in glaucoma.* Exp Eye Res, 2017. **158**: p. 3-12.

72. Raghunathan, V.K., et al., *Dexamethasone Stiffens Trabecular Meshwork, Trabecular Meshwork Cells, and Matrix.* Investigative ophthalmology & visual science, 2015. **56**(8): p. 4447-4459.
73. Zhang, Y., A.H. Conrad, and G.W. Conrad, *Effects of ultraviolet-A and riboflavin on the interaction of collagen and proteoglycans during corneal cross-linking.* J Biol Chem, 2011. **286**(15): p. 13011-22.
74. Rahman, N., et al., *Corneal Stiffness and Collagen Cross-Linking Proteins in Glaucoma: Potential for Novel Therapeutic Strategy.* J Ocul Pharmacol Ther, 2020. **36**(8): p. 582-594.
75. Ahearne, M. and A. Coyle, *Application of UVA-riboflavin crosslinking to enhance the mechanical properties of extracellular matrix derived hydrogels.* J Mech Behav Biomed Mater, 2016. **54**: p. 259-67.
76. Heo, J., et al., *Riboflavin-induced photo-crosslinking of collagen hydrogel and its application in meniscus tissue engineering.* Drug Deliv Transl Res, 2016. **6**(2): p. 148-58.
77. Tirella, A., T. Liberto, and A. Ahluwalia, *Riboflavin and collagen: New crosslinking methods to tailor the stiffness of hydrogels.* Materials Letters, 2012. **74**: p. 58-61.
78. Makita, R., et al., *Multiple renal cysts, urinary concentration defects, and pulmonary emphysematous changes in mice lacking TAZ.* Am J Physiol Renal Physiol, 2008. **294**(3): p. F542-53.
79. Morin-Kensicki, E.M., et al., *Defects in yolk sac vasculogenesis, chorioallantoic fusion, and embryonic axis elongation in mice with targeted disruption of Yap65.* Mol Cell Biol, 2006. **26**(1): p. 77-87.
80. Hossain, Z., et al., *Glomerulocystic kidney disease in mice with a targeted inactivation of Wwtr1.* Proceedings of the National Academy of Sciences, 2007. **104**(5): p. 1631-1636.
81. Toyama, T., et al., *Therapeutic Targeting of TAZ and YAP by Dimethyl Fumarate in Systemic Sclerosis Fibrosis.* J Invest Dermatol, 2018. **138**(1): p. 78-88.
82. Akimov, S.S., et al., *Tissue transglutaminase is an integrin-binding adhesion coreceptor for fibronectin.* The Journal of cell biology, 2000. **148**(4): p. 825-838.
83. Lin, C., et al., *YAP is essential for mechanical force production and epithelial cell proliferation during lung branching morphogenesis.* Elife, 2017. **6**.
84. Nardone, G., et al., *YAP regulates cell mechanics by controlling focal adhesion assembly.* Nature Communications, 2017. **8**(1): p. 15321.
85. Mason, D.E., et al., *YAP and TAZ limit cytoskeletal and focal adhesion maturation to enable persistent cell motility.* J Cell Biol, 2019. **218**(4): p. 1369-1389.
86. Qiao, Y., et al., *YAP Regulates Actin Dynamics through ARHGAP29 and Promotes Metastasis.* Cell Rep, 2017. **19**(8): p. 1495-1502.